Direct Use of Mixing Data for Modeling High-Viscosity, Melt-Phase, Condensation Polymer Reactors

SWATI NEOGI and KENDREE J. SAMPSON*

Department of Chemical Engineering, Ohio University, Athens, Ohio 45701

SYNOPSIS

Mathematical models for simultaneous reaction and mass transfer occurring in the manufacture of high-viscosity condensation polymers are considered. Particle tracking experiments are used to estimate convective flow rates and mixing volumes in a disc-ring reactor configuration. These results are incorporated directly into a mixing-cell model without resorting to the use of restrictive assumptions regarding the convective mixing. Both a penetration theory model and a flash evaporation model are used to simulate the transport at the liquid–vapor interface. Although widely used in previous studies, the penetration theory model is ultimately rejected because it underpredicts the overall reactivity. Model results predict interactions between agitation rate, residence time, and the overall reaction rate for commercial-scale systems producing poly(ethylene terephthalate). The model is partially verified by comparison with degassing data. © 1995 John Wiley & Sons, Inc.

INTRODUCTION

Manufacture of condensation polymers in a melt-phase process often requires continuous removal of the condensation product from the reaction mass to drive the reaction to high conversion. This occurs when the polycondensation reaction is reversible. At high conversion, the high viscosity of the melt decreases the rate of transport of the condensation product to the liquid surface and thereby reduces the overall reaction rate. A primary reactor design problem is to generate large amounts of surface area within the polymerization reactor in order to reduce the effective distance over which the condensation product must diffuse. A second problem is to ensure adequate mixing between the bulk of the reaction mass and the surface. This design challenge is currently met using a variety of equipment configurations. Examples of commercial polycondensation reactor designs include twin-screw and multiple-screw extruders, twin-shaft paddle mixers, horizontal disc-ring reactors, and the more traditional (and less capable) stirred tank with an anchor agitator.

The interconnection of the mass-transfer problem and kinetic phenomena poses a serious challenge to modeling these reactors. The problem is aggravated by the fact that the mass-transfer rate of the condensation product is a function of both the diffusivity of the condensation product and the convective mixing. A fundamental understanding of the melt-phase polycondensation process is required to enable improved methods for design, scale-up, and operation of commercial reactors. This need is magnified by current trends in commercial polymer product development, which include manufacture of increasingly high-viscosity polymers, use of low diffusivity condensation products, and development of more thermally sensitive polymer products.

In a previous article,[1] the authors showed that several diverse models describing combined reaction and mass transfer in condensation polymer reactors can be represented by a single formula based upon an effectiveness factor. They considered models by Ault and Mellichamp[2] and Ravindranath and Mashelkar[3] as well as three original forms. They also developed a general modeling framework based upon a mixing-cell concept and showed that the new framework can be represented by an effectiveness factor form and can be used to span the predictions generated by the previous models.

* To whom correspondence should be addressed.

Journal of Applied Polymer Science, Vol. 55, 761–772 (1995)
 CCC 0021-8995/95/050761-12

The objective of this article was to further the development by estimating model parameters directly from mixing experiments. The general framework is retained while being applied to a specific system with complicated flow patterns. The results remain free from restrictive assumptions since the fluid motion itself is used to define the structure of the mixing cells in the model.

The starting point of this research is the generation of mixing data from experiments that simulate the convective mixing pattern of a commercial melt-phase polycondensation reactor. The disc-ring reactor configuration has been chosen for the study and has been scaled-down to a laboratory-scale mixer. A model fluid that simulates the rheological behavior of the polymer melt is used in the mixer. The flow pattern of a particle embedded in the fluid is studied. Observation of the flow pattern leads to a conceptual discretization of the flow field into a few mixing cells. Mixing data generated in the experiment consist of a record of cells through which the particle travels and the times when it moves from one cell to another. These data are used to calculate the flow rates between each pair of cells and the volumes of the cells. The intercell flow rates and cell volumes are then used to develop a model that includes the combined effects of reaction and convective mixing and that predicts the overall reaction rate in a commercial-size vessel. This model is referred to in what follows as the multiple-cell model.

To demonstrate that mixing in the bulk causes a significant effect on reactor performance, another mixing-cell model, referred to as the two-cell model, has been developed. In the two-cell model, mixing between regions in the bulk liquid pool is assumed to be instantaneous. The structure of this model is similar to the multiple-cell model. Either form represents an improvement on the traditional well-mixed or continuous-stirred-tank-reactor (CSTR) model, which, in the nomenclature used here, would be a single-cell model.

In addition to the reaction and convective mixing processes referred to above, a key feature of this process is the devolatilization of condensation product at the liquid–vapor interface. A penetration theory model has been rejected due to the unrealistically low overall reaction rates predicted by this approach. In its place, a flash evaporation model is postulated.

Finally, an experimental procedure has been developed to partially verify the mixing-cell model by measuring the rate of degassing of carbon dioxide from the simulation fluid. The mixing-cell models (both the multiple- and two-cell models) have been modified to simulate the nonreactive degassing experiment and the simulated data are compared with the experimental data.

MIXING EXPERIMENTS

The experimental mixing apparatus simulates a commercial disc-ring reactor. It consists of a transparent horizontal cylinder with a single disc mounted on a horizontal shaft running through the center of the chamber. A sketch of the apparatus is shown in Figure 1. The chamber is partially filled with an aqueous solution of polyacrylamide that matches (at room temperature) the viscosity of molten poly(ethylene terephthalate) and is transparent enough to permit the tracking of an opaque particle embedded in the fluid using a video camera

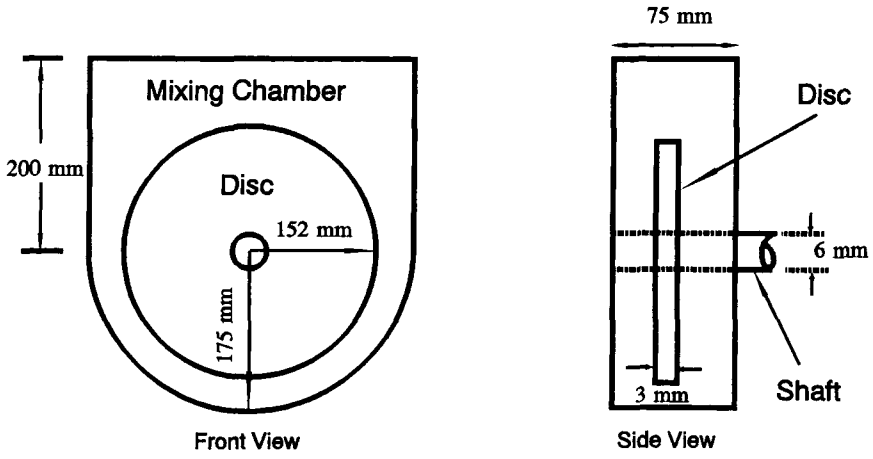

Figure 1 Schematic of the mixing apparatus.

and recorder. The mixing experiment setup is described in Figure 2.

The number and arrangement of mixing cells is determined based upon qualitative observations of the flow pattern in the apparatus. The discretization pattern found in these experiments is shown in Figure 3. The velocity of the particle in the liquid pool near the disc (cells 1 and 2 in Fig. 3) is much higher than is the velocity away from the disc (cell 3 in Fig. 3). The region of the disc exposed to the vapor space above the liquid is designated as cell 1. The submerged portion of the disc is designated as cell 2. The particle moves between cell 1 and cell 2 several times before leaving this region. As it circles around the disc, the particle moves toward the center of the disc and eventually falls off of the disc and enters cell 3. Although this same pattern was observed in these experiments for all disc rotation rates and fluid levels, it is likely that other patterns would be found if more extensive changes in the configuration or operating conditions were made.

The discretization pattern shown in Figure 3 is translated into the arrangement of mixing cells shown in Figure 4. The location of feed and product streams is somewhat arbitrary. For the specific application at hand, cell 3 is used; both cells 2 and 3 would be reasonable choices. The location affects the reactive simulations but has no impact on the mixing experiments themselves. It is assumed that the flow between cells is at a steady state. The linear arrangement of cells shown in Figure 4 then implies that the flow rate between any two cells must be the same in both directions.

The mixing data, which consists of the record of mixing cells through which the particle moves and the times when it moves from cell to cell, can be used to calculate the volume of each mixing cell and the intercell flow rates. Only the total volume of the liquid must be known beforehand.

The mean residence time of the fluid in a cell is assumed to be the same as that of the particle. The experimental mean residence time of the particle in cell j is given by

$$\tau_{m,j} = \frac{1}{m_j} \sum_{p=1}^{m_j} (t_{i,jp} - t_{0,jp}) \tag{1}$$

where $t_{i,jp}$ and $t_{0,jp}$ are the times the particle enters and exits cell j corresponding to the pth observation for cell j, and m_j is the number of observations for cell j. If V_j is the volume of mixing cell j, then the total flow rate, $Q_{0,j}$, entering or leaving cell j is related to the mean residence time by

$$Q_{0,j} = \frac{V_j}{\tau_{m,j}} \tag{2}$$

The flow from cell j to cell k is the total flow out of cell j times the fraction of the total flow leaving cell j that enters cell k or the total flow into cell k times the fraction of the total flow entering cell k that comes from cell j. Assuming that the flow rates between cells are proportional to the frequency of movement of the particle between cells,

$$Q_{jk} = Q_{0,j} \frac{n_{j,k}}{\sum_{l=1,j}^{n_M} n_{j,l}} = Q_{0,k} \frac{n_{j,k}}{\sum_{l=1,k}^{n_M} n_{l,k}} \tag{3}$$

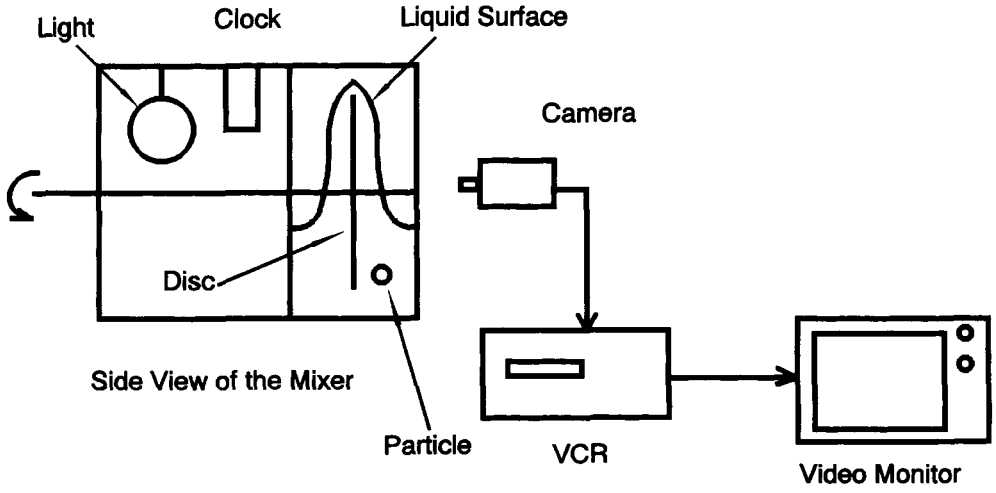

Figure 2 Configuration of the equipment used in the mixing experiments.

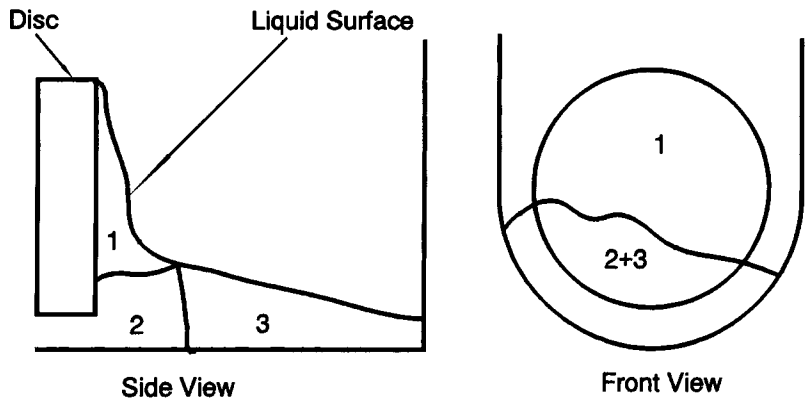

Figure 3 Discretization pattern found from the experimental mixing studies.

In eq. (3), Q_{jk} is the flow rate from cell j to cell k; n_M, the number of mixing cells; and $n_{j,k}$, the number of times the particle travels from cell j to cell k.

After substituting eq. (2) into eq. (3), the following relationship can be derived for the ratio of the volumes of any two mixing cells:

$$\frac{V_j}{V_k} = \frac{\tau_{m,j}}{\tau_{m,k}} \frac{\sum_{l=1,j}^{n_M} n_{j,l}}{\sum_{l=1,k}^{n_M} n_{l,k}} \tag{4}$$

The volume of cell j can then be related to the volume ratios given in eq. (4) and the total volume of all the mixing cells by

$$V_j = \frac{V_M}{\sum_{k=1}^{n_M} \frac{V_k}{V_j}} \tag{5}$$

where V_M is the total volume of fluid in the reactor.

The volume of each mixing cell and the intercell flow rates obtained for the laboratory mixer have been scaled up for a commercial-scale reactor and incorporated into the reactive simulation described in the next section. The scale-up has been achieved by maintaining geometric and dynamic similarity between the two reactors.[4] The following equations are used to scale-up the mixing data:

$$\bar{V}_j = V_j(\bar{D}_R/D_R)^3 \tag{6}$$

$$\bar{A}_s = A_s(\bar{D}_R/D_R)^2 \tag{7}$$

$$\bar{N} = N(\bar{D}_R/D_R)^{-0.5} \tag{8}$$

and

$$\bar{Q}_{jk} = Q_{jK}(\bar{D}_R/D_R)^{2.5} \tag{9}$$

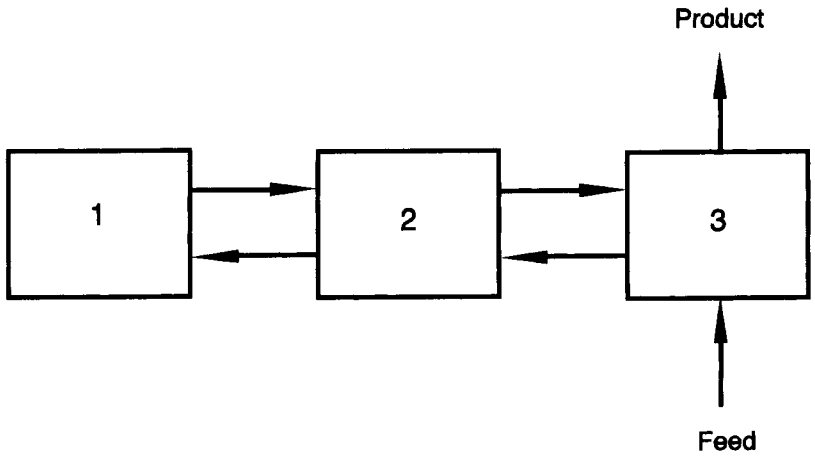

Figure 4 Intercell flow patterns derived from discretization shown in Figure 3.

In the above equations, the variables with the bar are the scaled-up variables. D_R is the reactor diameter; A_s, the exposed surface area on the disc; and N, the shaft speed. Equations (6) and (7) maintain the geometric similarity. Equations (8) and (9) maintain a constant Froude number and Reynolds number during scale-up.

The intercell flow rates calculated by the method described above apply to both batch and continuous flow systems. As long as the flow rate from outside the system into any given cell is the same as the flow rate leaving the system from the same cell, and as long as the flow rates into and out of the system are low enough to ignore inertial effects, the intercell flow rates will be unaffected.

REACTIVE SIMULATIONS

Amon and Denson[5] and Ault and Mellichamp[6] developed models for wiped-film reactors assuming that the bulk is well mixed and that the film entering the liquid pool mixes with the pool completely. Murakami et al.[7] used the same approach for a disc-ring reactor. Applying the same type of analysis in a different chemical system, Ravetkar and Kale[8] and Yamane and Yoshida[9] also assumed that the film mixed perfectly with the bulk liquid when modeling gas absorption into low viscosity liquids using a disc-ring contactor. More recently, Suga and Boongorsrang[10] recognized the importance of the limited mixing between the liquid film and the bulk liquid and developed a model based upon a boundary layer analysis of the submerged liquid near the disc.

In more recent articles, Laubriet et al.[11] and Saint Martin and Choi[12] developed a comprehensive model for final polymer reactors by using a film resistance mass-transfer coefficient to describe the mass-transfer resistance. Convective mixing between the bulk and liquid film was not considered. Of particular relevance to this work, Saint Martin and Choi[12] also concluded that the use of penetration theory gives unrealistically low reaction rates.

The multiple-cell model developed here eliminates the need for restrictive mixing assumptions by letting the mixing data suggest the number and configuration of mixing cells. The bulk is divided into two cells in this work. More divisions may be needed in other configurations or with operating conditions not explored in this study. For the purpose of comparison, a two-cell model has also been developed. It assumes that the entire liquid pool is well mixed.

Both the multiple-cell and two-cell models assume that a fraction of the bulk is continuously withdrawn as a film on the surface of the disc and that mass transfer of the condensation product occurs from the film to the surrounding vapor space. In this study, both a penetration theory model and a flash evaporation model are used to describe the transport from film to vapor. They are used in both the two-cell and multiple-cell models.

The penetration theory is based upon the concept originally put forth by Higbie.[13] This theory assumes that the time of exposure of a fluid to mass transfer is short so that the concentration gradient in the film does not have time to fully develop and the fluid behaves as a semi-infinite plane. This type of approach has been used previously by Ravindranath and Mashelkar,[3] Ault and Mellichamp,[2,6] Amon and Denson,[5] Secor,[14] and Murakami et al.[7] to model film-generating polycondensation reactors.

The operating pressure and temperature in a typical reactor used for the manufacture of poly(ethylene terephtalate) (PET) suggests the possibility of the formation of bubbles in the interior of the liquid. Since the static head in the liquid pool is often significant relative to the head space pressure, the concentration of the condensation product (ethylene glycol for the case of PET production) in the liquid may exceed the concentration in equilibrium with the vapor phase. The flash evaporization mechanism considered here assumes that the liquid withdrawn by the disc forms bubbles as the static head is removed and that the condensation product in the bubbles is removed spontaneously and instantaneously from the film as the bubbles collapse into the vapor–liquid interface. This assumption is essentially opposite from the penetration theory model and will overpredict the transport rate observed in practice due to its inherent idealizations.

Each cell is modeled as a CSTR with chemical reaction occurring in the cell. One could logically argue that both cells 1 and 2 would be better modeled as plug-flow reactors because the fluid adheres to the disc as it rotates; however, the practical distinction is minimal and the CSTR approach is more attractive because of its simplicity. The practical significance is low since the residence time of the fluid on the disc is much shorter than is the overall residence time of the fluid in the reactor. To substantiate this claim, a separate simulation has been performed approximating the plug-flow characteristics of cells 1 and 2 with a CSTR-in-series model containing 20 mixing cells or CSTRs. When the simulation with 20 cells is compared to the simulation with two cells, the largest difference observed

between them is a change in the predicted degree of polymerization (DP) from 57.3 to 57.6.

Transport occurs between cell 1 and the vapor space, among the cells, and between one cell and the feed and product streams. For the case of the penetration theory model, the cell with transport to the vapor is not modeled as a CSTR. Flow rates between mixing cells are based upon scale-up from the mixing experiments.

Development of the general model equations for a continuous flow system begins with the general polycondensation reaction

$$2S_1 \rightleftharpoons S_2 + S_3$$

where S_1 is a reactive end group; S_2, the polymer repeat unit; and S_3, the condensation product. The reaction rate expression is given by

$$r_j = kC_{1,j}^2 - \frac{4k}{K} C_{2,j}C_{3,j} \tag{10}$$

where $C_{i,j}$ is the liquid-phase concentration of the ith chemical component in the jth cell; k, the forward reaction rate constant; and K, the equilibrium constant. The rate of formation for the components in mixing cell j is given by

$$R_{1,j} = -2r_j \quad j = 1, 2, 3, \ldots, n \tag{11}$$

$$R_{2,j} = R_{3,j} = r_j \quad j = 1, 2, 3, \ldots, n \tag{12}$$

A general material balance equation governing the concentration of each species is given by

$$V_j \frac{dC_{i,j}}{dt} = \sum_{k=1}^{n} [Q_{kj}C_{i,k} - Q_{jk}C_{i,j}] + R_{i,j}V_j \qquad i = 1, 2, 3 \tag{13}$$

A transient form of the equations is presented here even though the steady-state solution is desired. The steady-state solution is generated from the asymptotic behavior of the solution as time increases. This approach is computationally simpler than solving the nonlinear algebra problem associated with the steady-state formulation. Note that the cell volumes are assumed to be constant. Note also that the development beginning with eq. (13) applies to a general configuration of cells rather than the specific set of three cells found in the mixing experiments and that a distinct form is required in some cases as described below.

The material balance equation for the cell into which the feed is introduced and from which the product is withdrawn is given by

$$V_n \frac{dC_{i,n}}{dt} = \sum_{k=1}^{n} [Q_{kn}C_{i,k} - Q_{nk}C_{i,n}] + Q_0[C_{i,0} - C_n] + R_{i,n}V_n \qquad i = 1, 2, 3 \tag{14}$$

where $C_{i,0}$ is the concentration of the ith component in the feed, and Q_0, the volumetric flow rate of the feed and product streams. This cell has been designated as cell n.

The rest of the development diverges for the two different mass-transfer models. For the penetration theory, both the cell with transport to the vapor, cell 1, and the cell connected to it, cell 2, require special consideration. The material balance equation for any component in cell 2 is

$$V_2 \frac{dC_{i,2}}{dt} = \sum_{k=2}^{n} [Q_{k2}C_{i,k} - Q_{2k}C_{i,2}] + Q_{12}\hat{C}_{i,1} - Q_{21}C_{i,2} + R_{i,2}V_2 \qquad i = 1, 2, 3 \tag{15}$$

Equations (14) and (15) are distinguished by the fact that $\hat{C}_{i,1}$ is the average concentration of the ith component in the fluid coming from cell 1. Other cells are well mixed, in which case there is no distinction between $\hat{C}_{i,j}$ and $C_{i,j}$.

Using penetration theory, $\hat{C}_{i,1}$ is calculated by solving a diffusion and reaction equation for cell 1:

$$\frac{dC_{i,1}}{dt_e} = D_i \frac{d^2C_{i,1}}{dx^2} + R_{i,1} \quad i = 1, 2, 3 \tag{16}$$

Here, D_i is the diffusivity of the ith component; t_e, the exposure time on the exposed surface; and x, the distance from the surface of the film. Since the diffusion coefficients for polymer molecules are much smaller than that for the smaller condensation product molecule, we can approximate

$$D_1 = D_2 = 0 \tag{17}$$

Equation (16) becomes a first-order ordinary differential equation when eq. (17) is used for components 1 and 2; however, eq. (16) will still depend on x via the reaction term.

Approximating the film as a semi-infinite domain, the boundary conditions required to solve eq. (16) are

$$C_{i,1} = C_{i,2} \quad \text{for } x \geq 0,\ t_e = 0 \quad i = 1, 2, 3 \tag{18}$$

$$C_{3,1} = C_3^* \quad \text{for } t_e > 0,\ x = 0 \tag{19}$$

and

$$C_{3,1} = C_{3,2} \text{ for } t_e > 0,\ x = \infty \tag{20}$$

where C_3^* is the concentration of component i in equilibrium with the vapor. The average concentration of the ith component in the fluid element leaving cell 1 is given by

$$\hat{C}_{i,1} = \frac{1}{L}\int_0^L C_{i,1}|_{t_e=T_e}\, dx \quad i = 1, 2, 3 \tag{21}$$

where T_e is the total exposure time on the surface of the disc, and L, the film thickness.

Equations (13)–(15) need to be solved simultaneously using a numerical initial value method such as Runge–Kutta. Then, for each numerical time step, eqs. (16)–(21) must also be solved numerically. This approach requires excessive computational time and is susceptible to large numerical errors. To avoid this problem, a linearized penetration theory developed by Ravindranath and Mashelkar[3] is used here.

Using the linearized penetration theory, an expression for the average molar flux of the condensation product, N_{av}, is postulated as

$$N_{av} = [C_{3,2} - C_3^*]\sqrt{D_3 k_1} \quad \text{for } k_1 T_e > 10 \tag{22}$$

where

$$k_1 = \frac{4kC_{2,2}}{K} \tag{23}$$

Equation (22) is derived by assuming that the rate of formation of the condensation product (component 3) in the film is equal to the rate of desorption of the condensation product out of the film. This assumption implies that no reaction occurs in the rest of the mixing cells. The final penetration theory model used here does allow reaction to occur in other mixing cells. The significance of this contradiction is low. Trial computations that suppress the reaction in the other cells are almost indistinguishable from those that allow the reaction to occur.

Using eq. (22), the overall material balance equations for the three components in cell 1 are given by

$$Q_{21}C_{1,2} - Q_{12}\hat{C}_{1,1} = 2N_{av}A_s \tag{24}$$

$$Q_{21}C_{2,2} - Q_{12}\hat{C}_{2,1} = -N_{av}A_s \tag{25}$$

and

$$Q_{21}C_{3,2} - Q_{12}\hat{C}_{3,1} = 0 \tag{26}$$

For component 1, the molar flux is multiplied by a factor of 2 because the rate of reaction of component 1 is equal to twice the rate of reaction of component 2 or component 3.

Substituting eqs. (24)–(26) into eq. (15) gives

$$V_2\frac{dC_{1,2}}{dt} = \sum_{k=2}^{n}[Q_{k2}C_{1,k} - Q_{2k}C_{1,2}] - 2N_{av}a_i + R_{1,2}V_2 \tag{27}$$

$$V_2\frac{dC_{2,2}}{dt} = \sum_{k=2}^{n}[Q_{k2}C_{2,k} - Q_{2k}C_{2,2}] + N_{av}a_i + R_{2,2}V_2 \tag{28}$$

and

$$V_2\frac{dC_{3,2}}{dt} = \sum_{k=2}^{n}[Q_{k2}C_{3,k} - Q_{2k}C_{3,2}] + R_{3,2}V_2 \tag{29}$$

The flash evaporization mechanism requires different material balances for cells 1 and 2. It is assumed that the material flowing into the cell is supersaturated with the condensation product and that vapor bubbles are formed and escape from the liquid as soon as the fluid enters the cell. The concentration of condensation product throughout the cell is set by the vapor–liquid equilibrium:

$$C_{3,1} = C_3^* \tag{30}$$

Since cell 1 is modeled as being well mixed, the governing equations for components 1 and 2 are

$$V_1\frac{dC_{i,1}}{dt} = \sum_{k=1}^{n}[Q_{k1}C_{i,k} - Q_{1k}C_{i,1}] + R_{i,1}V_1 \quad i = 1, 2 \tag{31}$$

In this case, eq. (13) will be applicable to cell 2 along with the other cells.

The same modeling principles described above are applied to develop the two-cell model. The only difference is the number of cells. The feed is introduced into cell 2 and the product is withdrawn from cell 2. The volume of cell 2 is equal to the total volume of all mixing cells excluding the volume of cell 1.

Results from both the multiple-cell model and two-cell model, using both penetration theory and

flash evaporization mechanisms, are presented in Figures 5–7. Results are expressed in terms of the degree of polymerization. The two-cell and multiple-cell models with the flash evaporization mechanism are identified as Model 1 and Model 2, respectively. The two-cell and multiple-cell models with penetration theory are referred to as Model 3 and Model 4, respectively.

Reaction and physical property parameters correspond to a typical PET manufacturing process. These include a rate constant (k) of 0.1 m^3/kmol/s compared to a range of $9.17 \cdot 10^{-5}$ to 0.152 m^3/kmol/s reported by Stevenson and Nettleson,[15] an equilibrium constant (K) of 0.5 compared to a range of 0.5 to 1 used by Ravindranath and Mashelkar,[16] an operating pressure of 0.0656 kN/m^2 (0.5 Torr) compared to a range of 0.0656 to 0.137 kN/m^2 described by Ravindranath and Mashelkar,[17] a temperature of 553 K (280°C), and a diffusivity of the condensation product of $1.6 \cdot 10^{-8}$ m^2/s compared to a range of $8.2 \cdot 10^{-9}$ m^2/s reported by Rafler et al.[18] to $1.6 \cdot 10^{-8}$ m^2/s reported by Pell and Davis.[19] The vapor pressure of ethylene glycol is calculated using a correlation given by Fontana.[20] The intercell flow rates and surface areas are calculated based on the results from the mixing experiments and are scaled-up to a 2.4 m diameter reactor. The intercell flow rates and surface areas depend on the shaft speed and the volume of the fluid in the reactor.

Figure 5 shows the effect of shaft speed on the performance of a commercial PET reactor for a feed DP of 50 and a residence time of 2.5 h. The DP of the product increases as the shaft speed increases but levels off at high rpm's. The change in DP between the multiple-cell and two-cell models for the case of the penetration theory model is smaller than for the case of the flash evaporization mechanism. The difference between the multiple-cell model and the two-cell model for both the flash evaporization mechanism and the penetration theory models decreases as the rotation rate increases.

Differences between the two-cell and multiple-cell models can be explained qualitatively by the fact that the change in DP depends on the resistance to transport within the bulk, from the bulk to the surface, and from the surface to overhead vapor. The multiple-cell model recognizes the resistance to transport within the bulk whereas the two-cell model does not. This effect is less pronounced for the penetration theory (Models 3 and 4) where the resistance from the disc to the vapor space dominates. The DP predicted by the models with the flash evaporization mechanism is higher than that predicted by the models with the penetration theory, because in the former case, there is no resistance to mass transfer from the surface. As the rotation rate increases, the bulk becomes more well mixed and the resistance to transport within the bulk diminishes.

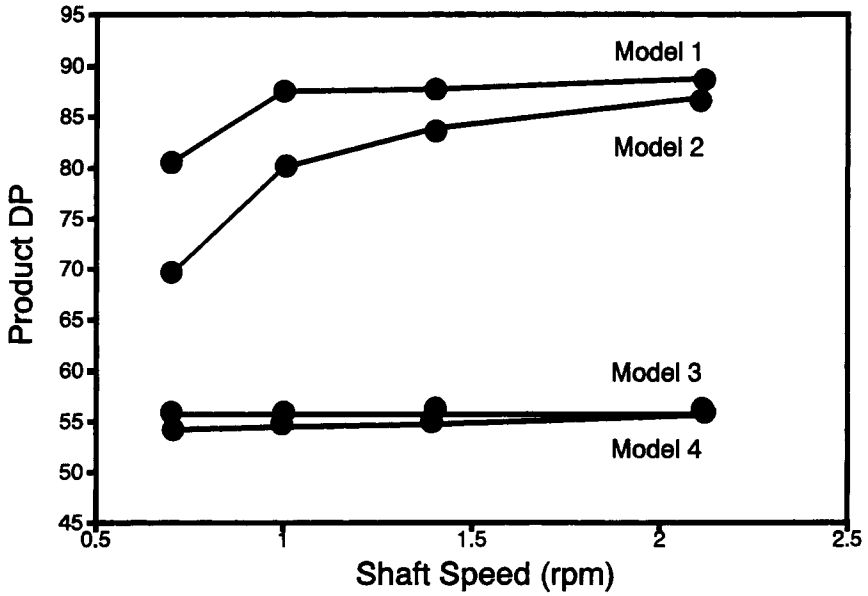

Figure 5 Effect of shaft speed on product DP. Feed DP is 50. Residence time is 2.5 h. The two-cell and multiple-cell models with the flash evaporization mechanism are identified as Model 1 and Model 2, respectively. Model 3 and Model 4 refer to the two-cell and multiple-cell models with the penetration theory, respectively.

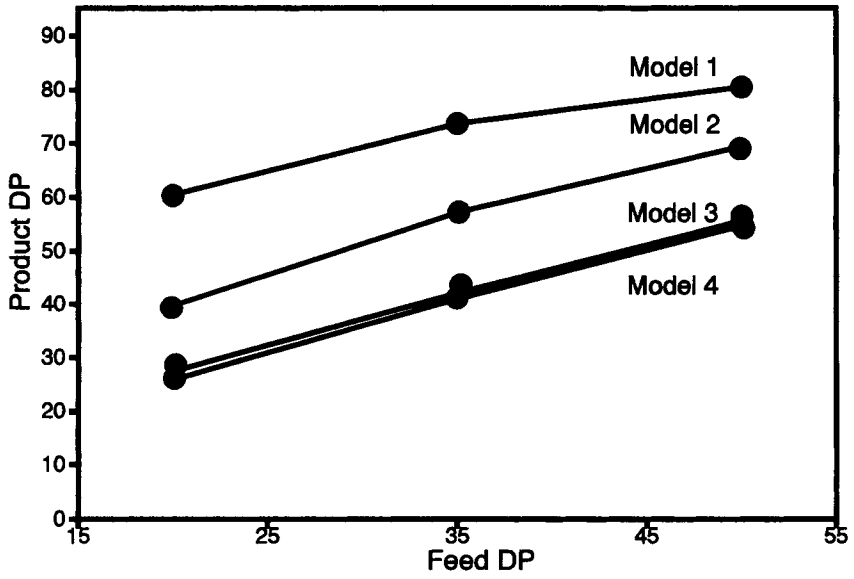

Figure 6 Effect of feed DP on product DP. Shaft speed is 2.12 rpm. Residence time is 2.5 h. The two-cell and multiple-cell models with the flash evaporization mechanism are identified as Model 1 and Model 2, respectively. Model 3 and Model 4 refer to the two-cell and multiple-cell models with the penetration theory, respectively.

This is the reason for the increase in product DP and the reduction in the difference between the two-cell and multiple-cell models as the rotational rate increases. In the limit as the shaft speed is increased, a single-cell CSTR model is realized. Figure 5 indicates the prediction for this limit to be a product DP of about 90.

Figure 6 shows the effect of the feed DP on the performance of the reactor. As before, the difference between the multiple-cell and two-cell models de-

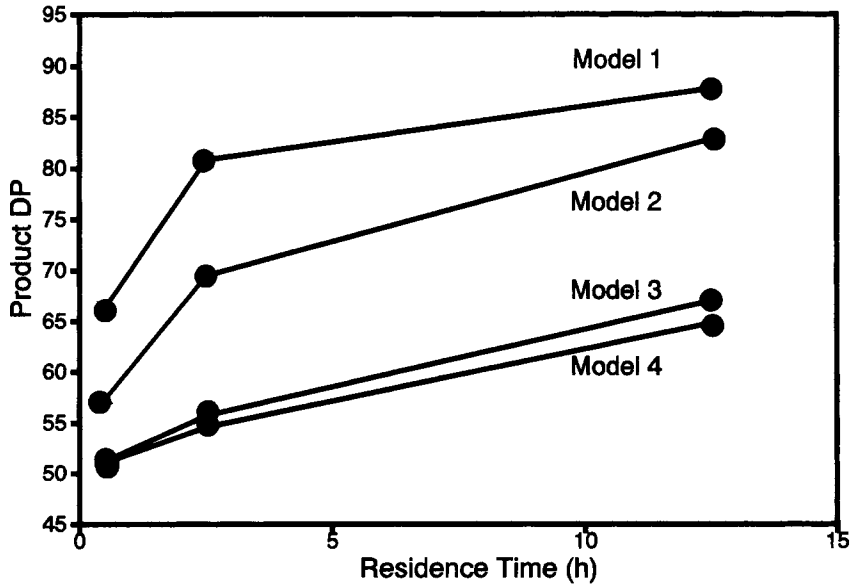

Figure 7 Effect of residence time on product DP. Shaft speed is 2.12 rpm. Feed DP is 50. The two-cell and multiple-cell models with the flash evaporization mechanism are identified as Model 1 and Model 2, respectively. Model 3 and Model 4 refer to the two-cell and multiple-cell models with the penetration theory, respectively.

creases as the shaft speed increases. The difference between the two types of models also decreases as the feed DP increases. This can be attributed to the fact that the same reactor pressure was used in all cases. This means that the results with higher feed DPs tend to approach reaction equilibrium more closely and thereby diminish the relative effect of the transport resistances.

The effect of residence time is demonstrated in Figure 7. Again, differences between the two-cell and multiple-cell models are more pronounced at the lower rotation rate. Also, once again, the model predictions tend to converge as reaction equilibrium is approached. Although it appears that the two penetration theory models diverge as the residence time is increased, the difference between the relative change in DP (between feed and product) actually decreases.

The results in Figures 5–7 consistently show that the penetration theory predicts an unrealistically low rise in the degree of polymerization (DP) for a typical reactor used in the PET manufacturing process. At the same time, the flash evaporation model gives reasonable results. For example, Yokoyama et al.[21] reported a DP rise from 50 to 100 in less than 1 h at 553 K (280°C) and 0.08 kN/m^2 (0.6 Torr) using a helical ribbon agitator. This suggests that the use of a penetration theory approach is inappropriate. This conclusion will be mitigated if commercial reactors achieve better mixing between the liquid pool and film or if bubbles formed when the static head is removed are entrained in the film returning to the liquid pool.

MODEL VERIFICATION

Reactive experiments have not been conducted as part of this study. Therefore, the model predictions have not been verified directly. Instead, the rate of degassing of dissolved carbon dioxide from the simulation fluid in the mixing apparatus has been compared to the predictions from a nonreactive model.

Degassing experiments were performed by first saturating the fluid in the mixing apparatus with carbon dioxide and then removing the carbon dioxide by sweeping nitrogen gas through the head space in the apparatus. The concentration in the outlet gas stream was measured using a carbon dioxide gas analyzer (Siemens Model Ultramat 21p) that can measure concentrations from 0 to 1000 ppm. The concentration of carbon dioxide is plotted against time in Figures 8 and 9 for two sets of experimental conditions. When the concentration of carbon dioxide in the exiting gas stream reached about 500 ppm, the flow rate of the nitrogen gas was lowered in order to maintain the response near the center of the analytical range. This caused the periodic sharp rise in the concentration of carbon dioxide.

Both the two-cell and multiple-cell models were used to predict the results from the degassing experiments. The model is analogous to the reactive

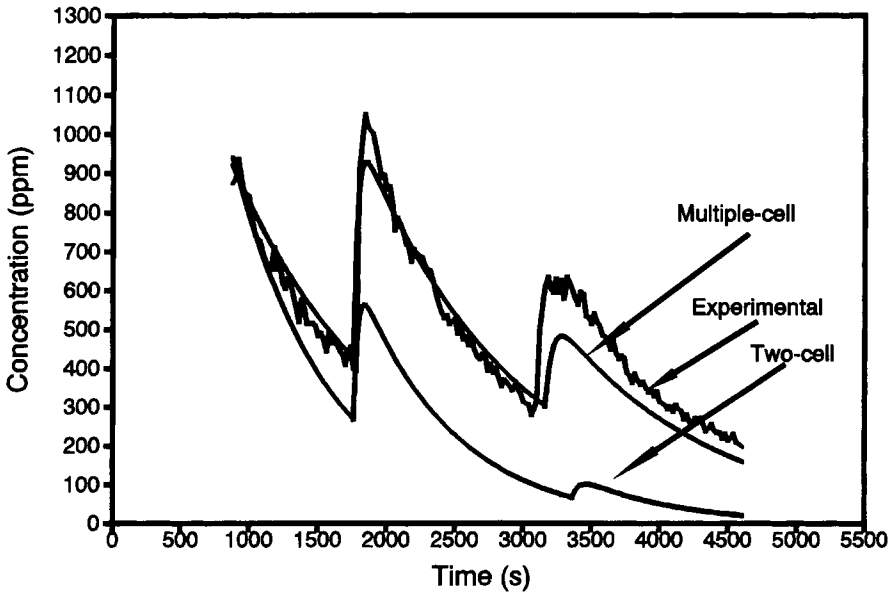

Figure 8 Comparison of the degassing data simulated by the two- and multiple-cell models with the experimental data for a shaft speed of 3 rpm, fluid volume of 1140 cm^3, and fluid viscosity of 57,500 cp.

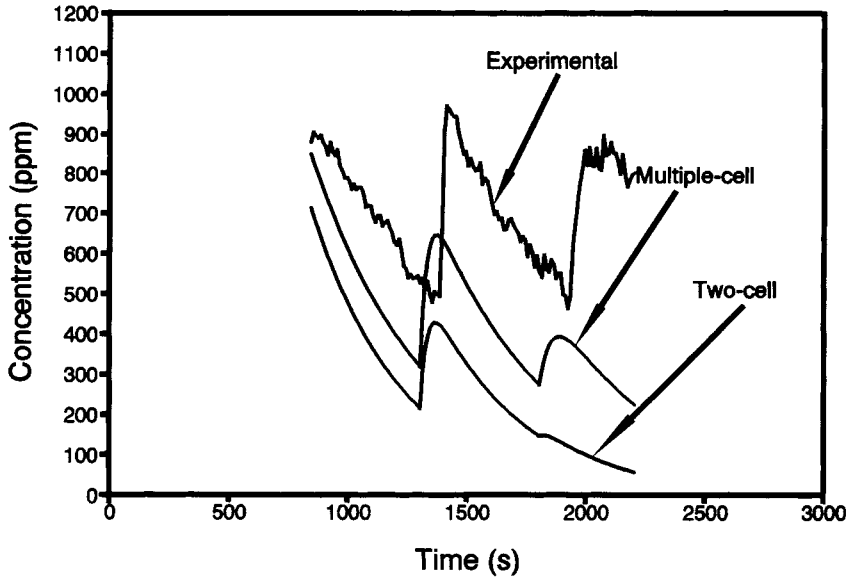

Figure 9 Comparison of the degassing data simulated by the two- and multiple-cell models with the experimental data for a shaft speed of 6 rpm, fluid volume of 1140 cm^3, and fluid viscosity of 57,500 cp.

simulations with the exceptions that the reaction terms are omitted, that penetration theory is used exclusively for cell 1, and that an additional mixing cell is included to model the behavior of the gas held inside the mixing apparatus. The material balance for cells 2 and 3 are

$$V_j \frac{dC_{4,j}}{dt} = \sum_{k=1}^{n} [Q_{kj}C_{4,k} - Q_{jk}C_{4,j}] \quad i = 2, 3 \qquad (32)$$

where the subscript 4 indicates carbon dioxide. The penetration theory model (without reaction) can be solved analytically to give

$$N_{av} = -[C_4^* - C_{4,2}]\sqrt{\frac{D_4}{\pi T_e}} \qquad (33)$$

The gas-phase mixing cell is governed by

$$V_g \frac{dC_{4,g}}{dt} = N_{av}A_s - Q_gC_{4,g} \qquad (34)$$

where the subscript g refers to the gas phase and Q_g is the flow rate of gas into and out of this cell.

Experimental values for the diffusion coefficient of carbon dioxide in an aqueous polyacrylamide solution have been reported up to a concentration of 0.3 wt %.[22,23] Under these conditions, the diffusivity is close to that in pure water. The value of diffusivity in pure water is $1.8 \cdot 10^{-9}$ m^2/s, whereas the maximum value in an aqueous polyacrylamide solution is $2.289 \cdot 10^{-9}$ m^2/s in the range of concentrations studied. The value for diffusivity of carbon dioxide in the fluid used in the simulation was taken as $2.0 \cdot 10^{-9}$ m^2/s based on these results. (The maximum concentration used in the mixing experiments was 2.4 wt % polyacrylamide.)

The results in Figures 8 and 9 represent the best and worst agreement between the experiments and the multiple-cell model among eight experimental trials reported elsewhere.[4] In either case, the agreement is acceptable and the distinction between the two-cell and multiple-cell models clearly favors the multiple-cell model. Among other possibilities, the disagreement between the experiments and multiple-cell model predictions may be due to inaccuracy in the diffusivity value, due to the assumption that the head space is well mixed, or due to the appearance of dead zones in the liquid volume. It is important to note that the appearance of dead zones cannot be established by the experimental technique used here since the particle being tracked will, by definition, not enter a dead zone.

CONCLUDING REMARKS

The approach presented in this article is a workable solution to a complex modeling problem. It is particularly attractive due to the fact that the mixing-cell configuration is established by the mixing data directly rather than by applying intuitive simplifications. This advantage comes at the price of having to generate mixing data. Although not completely

verified by experiment, the model predictions are useful. Limited mixing in the bulk liquid pool appears to have a significant impact on the overall reactivity in many cases.

NOMENCLATURE

- A_s surface area of the disc above the fluid level in the reactor
- $\bar{A}_s$ scaled-up surface area of the disc above the fluid level in the reactor
- C_3^* concentration of the ith component in equilibrium with the vapor
- $C_{i,0}$ concentration of the ith component in the feed
- $\hat{C}_{i,1}$ average concentration of the ith component in the fluid coming from cell 1
- $C_{i,j}$ liquid-phase concentration of the ith chemical component in the jth cell
- D_i diffusivity of the ith component
- $\bar{D}_R$ scaled-up diameter of a disc-ring reactor
- D_R diameter of the mixer
- k forward reaction rate constant
- k_1 dimensionless rate constant
- K equilibrium constant
- L film thickness on the disc
- m_j number of observations for cell j
- N shaft speed
- $\bar{N}$ scaled-up shaft speed
- N_{av} average molar flux of the condensation product
- n_M number of mixing cells
- $n_{j,k}$ number of times the particle travels from cell j to cell k
- Q_0 volumetric flow rate of the feed or product streams
- $Q_{0,j}$ total volumetric flow rate entering or leaving cell j
- Q_g volumetric flow rate of gas through the mixing apparatus
- Q_{jk} volumetric flow rate from cell j to cell k
- $\bar{Q}_{jk}$ scaled-up volumetric flow rate from cell j to cell k
- r_j reaction rate
- $R_{i,j}$ rate of formation of component i in mixing cell j
- S_1 reactive end group
- S_2 polymer repeat unit
- S_3 condensation product
- T_e total exposure time on the surface of the disc
- t_e current exposure time on the surface of the disc
- $t_{i,jp}$ time the particle enters cell j corresponding to the pth observation for cell j
- $t_{0,jp}$ time the particle exits cell j corresponding to the pth observation for cell j
- V_j volume of mixing cell j
- V_g volume of the gas in the mixing apparatus
- $\bar{V}_j$ scaled-up volume of mixing cell j
- V_M total volume of fluid in the reactor
- x distance from the surface of the film
- $\tau_{m,j}$ mean residence time of fluid in cell j

This material is based upon work supported by the National Science Foundation under Grant CBT-8808709. The U.S. Government has certain rights in this material. The authors express their appreciation for this support.

REFERENCES

1. K. J. Sampson, S. Neogi, and J. C. Medlin, *J. Appl. Polym. Sci.*, **47,** 1040 (1993).
2. J. W. Ault and D. A. Mellichamp, *Chem. Eng. Sci.*, **27,** 1441 (1972).
3. K. Ravindranath and R. A. Mashelkar, *Polym. Eng. Sci.*, **22,** 628 (1982).
4. S. Neogi, PhD Dissertation, Ohio University, 1993.
5. M. Amon and C. D. Denson, *Ind. Eng. Chem. Fund.*, **19,** 415 (1980).
6. J. W. Ault and D. A. Mellichamp, *Chem. Eng. Sci.*, **27,** 2233 (1972).
7. Y. Murakami, K. Fujimoto, S. Kakimoto, and M. Sekino, *J. Chem. Eng. Jpn.*, **5,** 257 (1972).
8. D. D. Ravetkar and D. D. Kale, *Chem. Eng. Sci.*, **36,** 399 (1981).
9. T. Yamane and F. Yoshida, *J. Chem. Eng. Jpn.*, **5,** 381 (1972).
10. K. Suga and A. Boongorsrang, *Chem. Eng. Sci.*, **39,** 767 (1984).
11. C. Laubriet, B. LeCorre, and K. Y. Choi, *Ind. Eng. Chem. Res.*, **30,** 2 (1991).
12. H. C. Saint Martin and K. Y. Choi, *Ind. Eng. Chem. Res.*, **30,** 1712 (1991).
13. R. Higbie, *Trans. AIChE,* **31,** 365 (1935).
14. R. M. Secor, *AIChE J.*, **15,** 861 (1969).
15. R. W. Stevenson and H. R. Nettleson, *J. Polym. Sci.*, **6,** 889 (1968).
16. K. Ravindranath and R. A. Mashelkar, *Developments in Plastic Technology-2,* Elsevier, London, 1985, p. 43.
17. K. Ravindranath and R. A. Mashelkar, *Chem. Eng. Sci.*, **41,** 2197 (1986).
18. G. Rafler, E. Bonatz, G. Reinisch, H. Gajewski, and K. Zacharias, *Acta Polym.*, **30,** 253 (1979).
19. T. M. Pell and T. G. Davis, *J. Polym. Sci.*, **11,** 1671 (1973).
20. C. M. Fontana, *J. Polym. Sci.*, **6,** 2343 (1968).
21. H. Yokoyama, T. Sano, T. Chijiwa, and R. Kajiya, *J. Jpn. Petrol. Inst.*, **21,** 58 (1978).
22. G. Astarita, *Ind. Eng. Chem. Fund.*, **4,** 236 (1965).
23. R. A. Mashelkar and M. A. Soylu, *Chem. Eng. Sci.*, **29,** 1089 (1989).

Received November 21, 1993
Accepted February 26, 1994